



A novel method for 3-D microstructure modeling of pome fruit tissue using synchrotron radiation tomography images

H.K. Mebatsion^{a,*}, P. Verboven^a, A. Melese Endalew^a, J. Billen^b, Q.T. Ho^a, B.M. Nicolai^{a,c}

^a BIOSYST – MeBioS, Katholieke Universiteit Leuven, Willem de Croylaan 42, B-3001 Leuven, Belgium

^b Department of Biology, Naamsestraat 59, 3000 Leuven, Belgium

^c Flanders Center of Postharvest Technology, Willem de Croylaan 42, B-3001 Leuven, Belgium

ARTICLE INFO

Article history:

Received 27 August 2008

Received in revised form 20 December 2008

Accepted 9 January 2009

Available online 29 January 2009

Keywords:

Transmission electron microscopy

Synchrotron radiation, computed tomography

Multiscale modelling

Finite element method

Cell, image processing, computational biology

ABSTRACT

Fruit microstructure determines mechanical and transport properties of tissues. This calls for geometric characterization and representation of fruit tissue components. In this paper, three important components of fruit cortex tissue, cell wall, pore network and cells were modeled in 3-D. These components were explicitly defined based on the information gathered from synchrotron X-ray computed tomography and transmission electron microscopy. The cells were modeled based on a novel ellipsoid tessellation algorithm, producing also 3-D void structures in small fruit cortex sample volumes. The cell wall thickness was determined from TEM images using digitization procedures. The resulting geometry models compared well to the tomographic images. The method has the significant advantages of, one, producing models that are easy to use in computer aided design software for multiscale mechanics and mass transfer, and two, providing a framework for virtual tissue generation, including cell growth modeling. Furthermore, the solid modeling approach avoids many problems of finite element meshing existing today.

© 2009 Elsevier Ltd. All rights reserved.

1. Introduction

Transport phenomena and mechanical deformation in plant tissues during food processing can be modeled using a model geometry assuming the plant tissue as a capillary-porous material consisting of liquid and gas phases (cells and intercellular spaces) and a solid matrix (the cell wall) (Lewicki and Pawlak, 2005). Therefore, in modeling a fruit structure to perform *in silico* experimentation, these three principal components should be defined and modeled precisely microscopically.

Fruits are composed of tissues that are anisotropic, heterogeneous, non-continuous and complex biological systems extending over nanoscopic to macroscopic length scales. The interconnection of neighboring protoplasts in tissues creates a continuous liquid network known as the symplast (Lewicki and Pawlak, 2005). The cell wall composed of mainly polysaccharides such as cellulose, hemicelluloses, pectin and lignin, along with proteins is the primary structural component of plants (Zhong and Ye, 2007). The perception of plant cell walls has evolved rapidly from early descriptions of inert, somewhat featureless boxes, to a currently accepted view of intricate highly dynamic structures with substan-

tial spatial and temporal variation in architecture and composition which resist both physical stresses and diseases (Lee et al., 2004; Jackman and Stanley, 1995). The networks of intercellular spaces form channels for gas transport needed for the respiratory metabolism. Verboven et al. (2008) measured 3-D void fraction and microscopic fruit structure in apple and pear by means of synchrotron radiation computed tomography. Intercellular spaces make up a significant fraction of a fruit ranging from 1% to 25% (Chaplain, 1993; Verboven et al., 2008). Even higher porosity values have been reported for apple cultivars such as Cameo (32%), Kanzi (28%) and Greenstar (28%) (Mebatsion et al., 2006a), based on 2-D micrographs. The volume of air space increases during fruit growth and occupies a considerable proportion of the fruit at harvest (Harker and Ferguson, 1988; Yamaki and Ino, 1992).

The porous structure of the tissue favors the action of hydrodynamic mechanisms in the pores due to capillary pressure and imposed or generated pressure gradients and diffusion in non-compartmented volumes such as intercellular spaces (Celia et al., 1995; Dražeta et al., 2004), or cells with denatured membranes. In plant organs, the gas filled intercellular spaces are the predominant pathways for gas transport (Kuroki et al., 2004; Mendoza et al., 2007). The volume of these intercellular air spaces continues to increase during fruit growth increasing the gas diffusion rates (Rajapakse et al., 1990; Ho et al., 2006). The cell wall allows the circulation and distribution of water, minerals, and other small nutrient molecules into and out of the cell via cell-to-cell interactions

* Corresponding author. Tel.: +32 16 32 05 90; fax: +32 16 32 29 55.

E-mail addresses: Hibru.Mebatsion@biw.kuleuven.be, hibruk@hotmail.com (H.K. Mebatsion).

(Chaplain, 1993). The symplast also involves in intercellular transport phenomena through plasmodesmatic actions (Denison, 1992).

Mebatsion et al. (2008a) reviewed the current state of the art in modeling tissue microstructures. What is currently lacking is a method to model the 3-D configuration of cells, cell walls and intercellular spaces in fruit tissues. With the recent breakthrough availability of accurate 3-D images of microstructures (Verboven et al., 2008), models can now be developed. This paper presents the application of a new modeling approach, based on tessellation algorithms (Mebatsion et al., 2008b) to model and quantify the different structural components of fruit cortex tissue, the major tissue of bulky fruit organs.

2. Materials and methods

2.1. Fruit

Pears (*Pyrus communis* cv. Conference) were harvested on September 13th, 2006, at the experimental station Fruitteelcentrum (Rillaar, Belgium). Apples (*Malus × domestica* Barkh cv. Jonagold) were picked on September, 25th, 2006, at the experimental station PCFruit (Velm, Belgium). All fruit were cooled and stored under controlled atmosphere conditions (2.5 kPa O₂, 0.7 kPa CO₂ –1 °C for pear; 1 kPa O₂, 2 kPa CO₂ –0.8 °C for apple).

2.2. Synchrotron radiation X-ray tomography of apple and pear cortex

The sample preparation and tomographic image acquisition procedures for pome fruit tissues outlined in Verboven et al. (2008) were employed. Cylindrical samples of 5 mm diameter and 1–2 cm length were removed from the different tissues of the fruits using a cork bore in the radial direction on the equator of the fruit. The samples were mounted in a polymethyl methacrylate tube and covered with polymer foil to avoid dehydration. Synchrotron X-ray CT of pear and apple fruit tissues was performed at the European Synchrotron Radiation Facility (ESRF), Grenoble, France. Beamline ID19 with a distance between the sample and camera of 35 mm was employed. Phase contrast images with a voxel size down to 700 nm were obtained. 2-D images were taken from different angular position over 180° of the sample in the basic process of microtomography. Tomographic reconstruction was performed with a filtered back projection algorithm using PyHST (ESRF) software. As a result, a series of slices that give detailed structural information about the 3-D nature of the material is acquired. Using phase contrast mode (Cloetens et al., 1999), this method allowed for the first time to clearly visualize micropores,

individual truncated ellipsoidal cells and cell walls, and their 3-dimensional connectivity. Fig. 1 shows tomographic slices of apple and pear parenchyma cells in the cortex. As can be seen in the figure, at 700 nm/pixel resolution it was possible to distinguish between the cells (elliptical shapes), the intercellular spaces (irregular darker regions between cells) and the cell wall between adjacent cells. Cell and void space separation on synchrotron images was performed manually in Avizo 5.0 (Mercury Computer Systems, Bordeaux, France). Six samples per fruit were analyzed to compare the geometrical characteristics of apples and conference pear tissue.

2.3. Transmission electron microscopy

While phase tomography allowed visualization of the 3-D position of cell walls in the tissue, the resolution was insufficient to measure cell wall thickness. Transmission electron microscopy (TEM) was used to further enhance resolution on separate samples for cell wall thickness estimation. New apples and pears for TEM were randomly chosen from storage containers under controlled atmosphere conditions (1% O₂, 2.6% CO₂ at 1 °C and 96% RH) stored for five months. The fruits were sliced into half and cylindrical samples were obtained from the cortex using a metallic bore. Very thin circular slices of about 1 mm thick were taken from these cylinders. The samples were immersed in ±400 µl glutaraldehyde fixative solution (2% 0.16 M sucrose in 0.06 M sodium cacodylate buffer, pH 7.4). The samples were kept under vacuum to pump the air out for about 15 min. Samples were then let at room temperature for about 24 h. Then, the fixation solution was carefully removed and replaced by buffer solution.

Samples passing through the initial treatment procedure were then post-fixed by osmium oxide in the same buffer, and dehydrated in a graded acetone series. They were then embedded in araldite. Semi-thin sections for light microscopy with a thickness of 5 µm were made with a Reichert Ultracut E microtome. Finally, cubic samples of about 1 mm side were obtained. Five samples per fruit were used for the analysis. Double stained thin sections with a thickness of 70 nm were examined in a Zeiss EM900 electron microscope. Chemicals and procedures for sample treatments were obtained from the Laboratory for Entomology of the K.U. Leuven, Leuven, Belgium.

Ultrastructural cell wall images were obtained using photographic plates. Using a digitizing procedure on the images in Matlab (The Mathworks, Natick, MA), the local and the mean cell wall thickness was determined (Fig. 2). We assume that averaging over a large number of samples resulted in a minimal error due to the

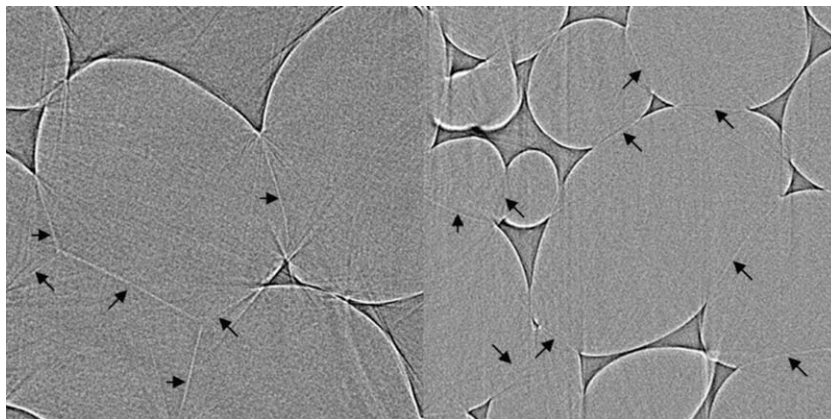


Fig. 1. Synchrotron radiation tomography: phase contrast slices of the fruit cortex of apple (cv. Jonagold, left) and pear (cv. Conference, right); cell walls are brightly highlighted (indicated by arrows).

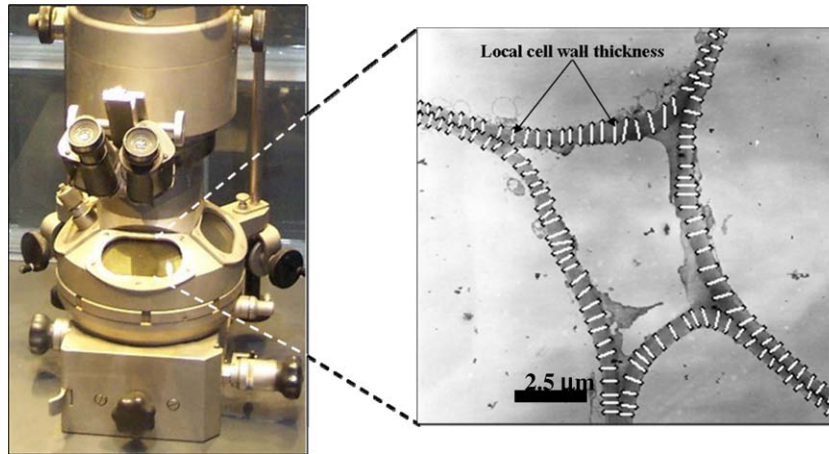


Fig. 2. Cell wall visualization in TEM (left) and local thickness measurement using the Matlab based digitization procedure (right) on the TEM image.

varying intercept angle of the section with respect to the plane of the cell wall. Cell wall thickness was $1.67 \pm 0.71 \mu\text{m}$ for apple and $0.77 \pm 0.51 \mu\text{m}$ for pear.

2.4. Digitization and ellipsoid tessellation algorithm

In the tomographic images, the differences in contrast between the pore space, the cell walls and the individual cells were too small for direct threshold segmentation (Verboven et al., 2008). Therefore a digitization procedure was implemented. The digitization was carried out manually using an in-house Matlab (The Mathworks, Natick, MA) based program. The coordinates of individual cells across a series of slices were estimated after the transformation of digital images to representative polygons defined by points on the natural boundaries of the cells. Once the three-dimensional coordinates of individual cells were established, ellipsoids that fit these sets of points were generated using a Least Squared Fitted Ellipsoid (LSFE) algorithm developed by Mebatsion et al. (2008b). Once LSFEs of individual cells were determined, the model tissue geometry was generated from the ellipsoids, which were truncated when neighboring volumes overlapped. As a result, as many truncated ellipsoids as there are cellular images were generated producing a virtual tissue that is representative of the fruit microstructure (Mebatsion et al., 2008b). Both digitization and ellipsoid tessellations were carried out with dedicated Matlab (The Mathworks, Natick, MA) routines. Fig. 3 shows the digitization and the LSFE procedures.

2.5. Geometry reconstruction of cells, intercellular spaces and cell walls

Individual ellipsoids representing individual cells of the tissue matrix were exported to ANSYS (ANSYS Inc., Canonsburg, PA) from the Matlab programming environment via interfacing Matlab code.

Matlab ellipsoid surface geometries were converted into standard IGES file format. Truncated solid ellipsoids resulted in aggregate cells consisting of non-overlapped volumes. The symplast was determined by the intersection of the total volume of the reconstructed region and the individual truncated ellipsoids. The intercellular spaces were determined from subtracting the symplast (V_s) from the total volume. The cell wall network was the collection of individual cell walls, which were obtained from subtracting shrunken ellipsoids from the original volumes, using the average cell wall thickness obtained from the TEM analysis.

3. Results

3.1. Geometric models of the fruit cortex

The modeled 3-D tissue architecture of apple and pear cortex samples is compared with the original synchrotron images (manually segmented into separate cells) in Figs. 4 and 5, respectively. The position, global shape and size of cells is matched accurately. We correctly find smaller cells in a denser pattern in pear cortex, compared to that of apple. The model is based on ellipsoids; therefore the cells appear smoother than in reality.

Based on the modeled cells, the void space was easily segmented from the total volume of the sample. The results of a single sample are compared to the void space in the original tissue images of apple and pear in Figs. 6 and 7, respectively. The differences in shape and size of voids between fruits are apparent in both model and reality: apple voids are large cavity structures, while in pear we find a network of small channels with throats as small as a few micrometers. As with the cells, the real pore space has a more distorted shape than modeled caused by the smooth sphericity of modeled cells. However, the connectivity of the void

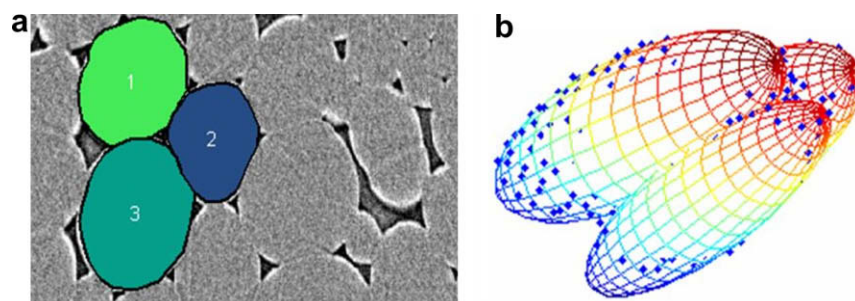


Fig. 3. The digitization of tomographic images (a) and the corresponding Least Squared Fitted Ellipsoids (LSFEs) (b).

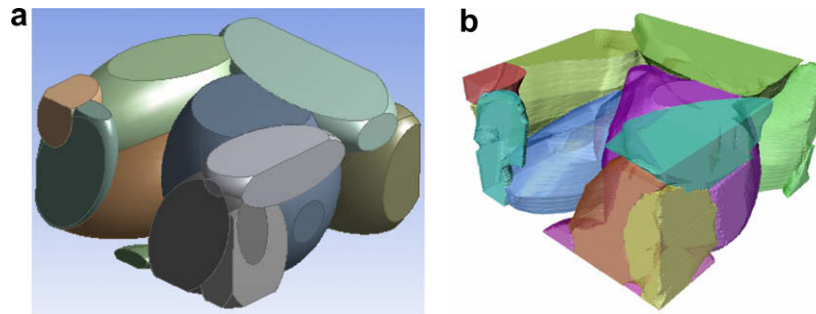


Fig. 4. Modeled (a) against measured (b) 3-D geometry of apple cortex cells. Sample dimensions were $315 \times 315 \times 168 \mu\text{m}$.

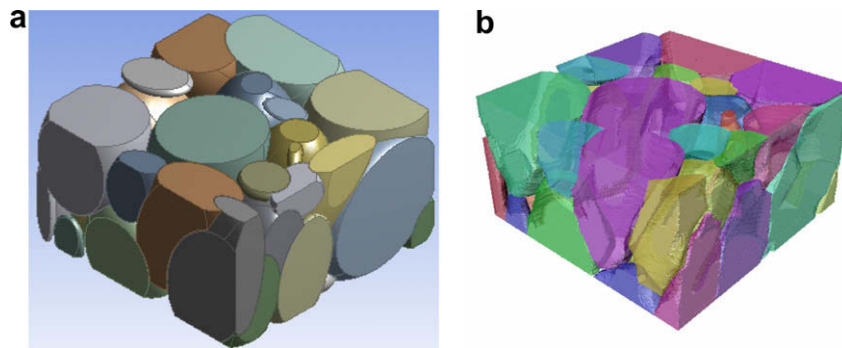


Fig. 5. Modeled (a) against measured (b) 3-D geometry of pear cortex cells. Sample dimensions were $315 \times 315 \times 168 \mu\text{m}$.

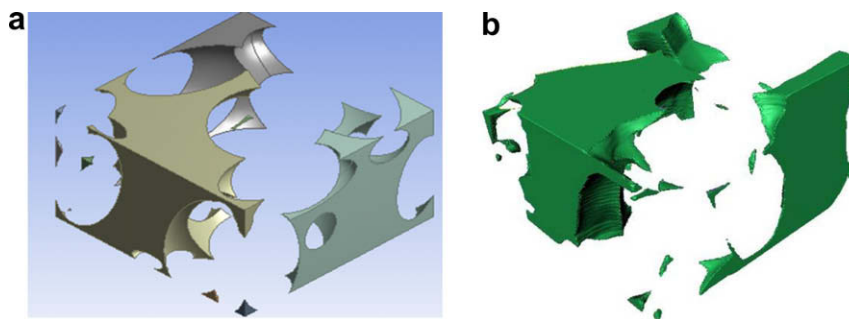


Fig. 6. Modeled (a) against measured (b) void space in an apple cortex sample. Sample dimensions were $315 \times 315 \times 168 \mu\text{m}$.

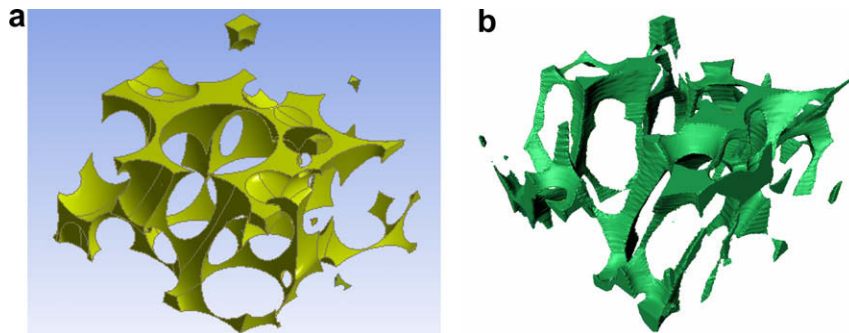


Fig. 7. Modeled (a) against measured (b) void space in a pear cortex sample. Sample dimensions were $315 \times 315 \times 168 \mu\text{m}$.

volumes was similar in measured and modeled samples. In the sample shown in Fig. 6, we find three large separate void volumes. For the pear sample in Fig. 7, apart from small isolated volumes at the edges of the sample, the entire void space is connected in a network pattern.

3.2. Structural characteristics of cortex tissue

The cumulative fractions of the real and modeled cell volumes in the apple and pear cortex tissue samples, which were discussed above, are compared in Fig. 8. We found more and smaller cells in

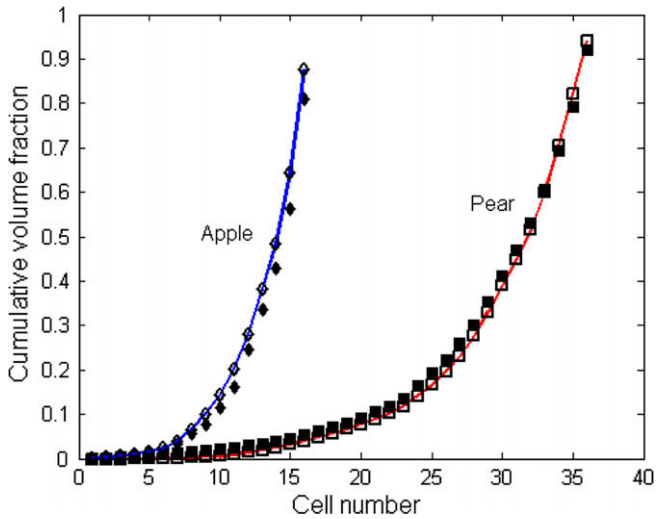


Fig. 8. Cumulative volume fraction of cells in cortex tissue samples of $315 \times 315 \times 168 \mu\text{m}$: solid symbols, measurement; line with symbols, model.

pears (36 against 16), and the distributions of real and modeled samples coincide very well. Note that these distributions include cut cells at the surfaces of the sample, and are therefore biased towards small cells. From the curves in Fig. 8, we can also calculate that the void fraction of the shown apple sample was 19%, the pear sample consisted only for 8% of voids. The corresponding values obtained from the models were smaller: 12% for apple, 6% for pear. The average void fractions of the different modeled apple and pear cortex tissue samples were determined to be $15.0 \pm 9.2\%$ and $11.1 \pm 2.5\%$, respectively.

In Fig. 9, we present the probability density functions of the modeled cell volumes over the total of 6 samples that were modeled. The apple cortex contains larger cells whereas the pear cortex contains lots of smaller cells. These distributions include cut cells at the surface of the samples, and are therefore biased to small volumes. The mean volumes of apple and pear parenchyma cells were calculated to be $6.39 \pm 7.76 \times 10^5 \mu\text{m}^3$ and $2.42 \pm 3.18 \times 10^5 \mu\text{m}^3$, respectively; this corresponds to an apparent mean diameter of 107 and 77 μm for apple and pear cortex, respectively. There was a significantly larger range of apple cell sizes than that of pear.

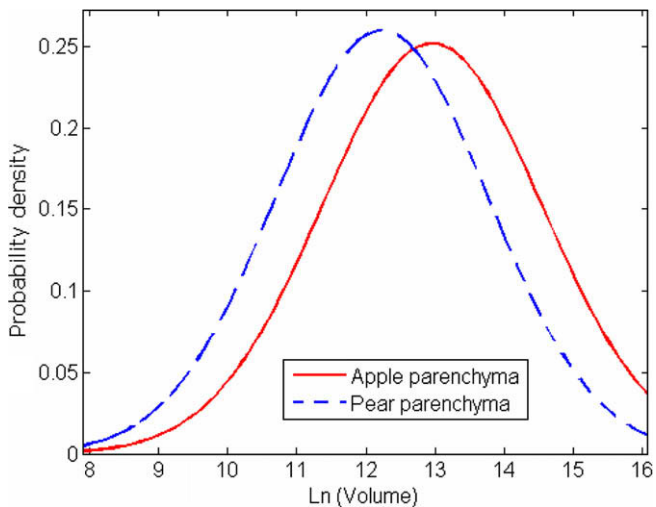


Fig. 9. Probability density function of modeled cell volumes (in μm) in apple and pear cortex tissue. Weibull distributions were fitted to the data for ease of comparison (Mebatsion et al., 2006). These distributions include cut cells at sample edges, therefore are biased towards smaller volumes.

The topological variation of the fruit tissues can be defined in terms of the number of first neighbors, also termed coordination number (Mebatsion et al., 2008b). The coordination numbers were 2.95 ± 1.97 and 4.31 ± 2.13 for apple and pear cortex tissues, respectively. The coordination number distribution is presented in Fig. 10. Clearly, the average coordination number of the larger apple cells is smaller than that of the pear cells.

3.3. From geometry model to a physical model of tissue

Figs. 11 and 12 present the modeled geometry of cortex tissue samples of apple and pear fruit, respectively, distinguishing the 3-D void space, cell walls, and symplast. Here we made use of the TEM analysis of cell wall thickness to shrink individual cells and obtain the cell wall network. Thicker cell walls appear in apple, as measured by TEM and apparent on the synchrotron images of Fig. 1. These are the first realistic geometrical models of the 3-D fruit microstructure that can be used in a computational framework, to our knowledge. The geometric models were exported into a finite volume mesher to create a computational mesh consisting of 6,539,231 tetrahedral elements as shown in Fig. 13; The zoomed view shows that excellent mesh quality is possible in the cell walls and at phase interfaces.

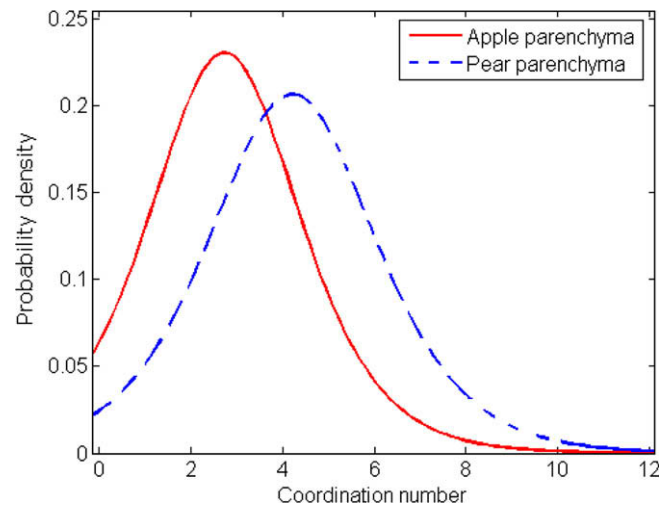


Fig. 10. The coordination number distribution of apple and pear parenchyma cells in modeled cortex samples. Logistic distributions were fitted to the data for ease of comparison (Mebatsion et al., 2006).

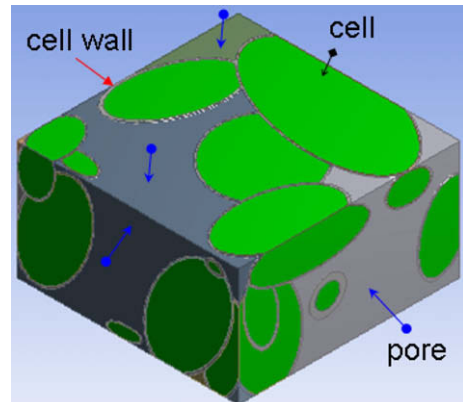


Fig. 11. Complete microstructure model of an apple cortex tissue sample. Sample dimensions were $315 \times 315 \times 168 \mu\text{m}$.

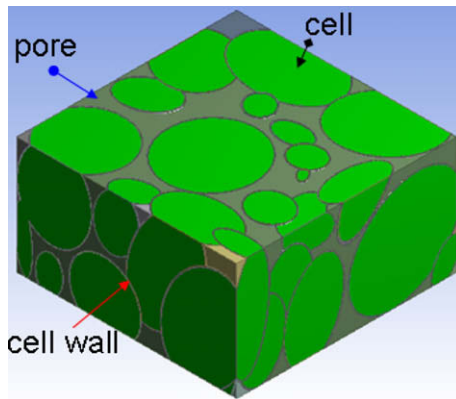


Fig. 12. Complete microstructure model of a pear cortex tissue sample. Sample dimensions were $315 \times 315 \times 168 \mu\text{m}$.

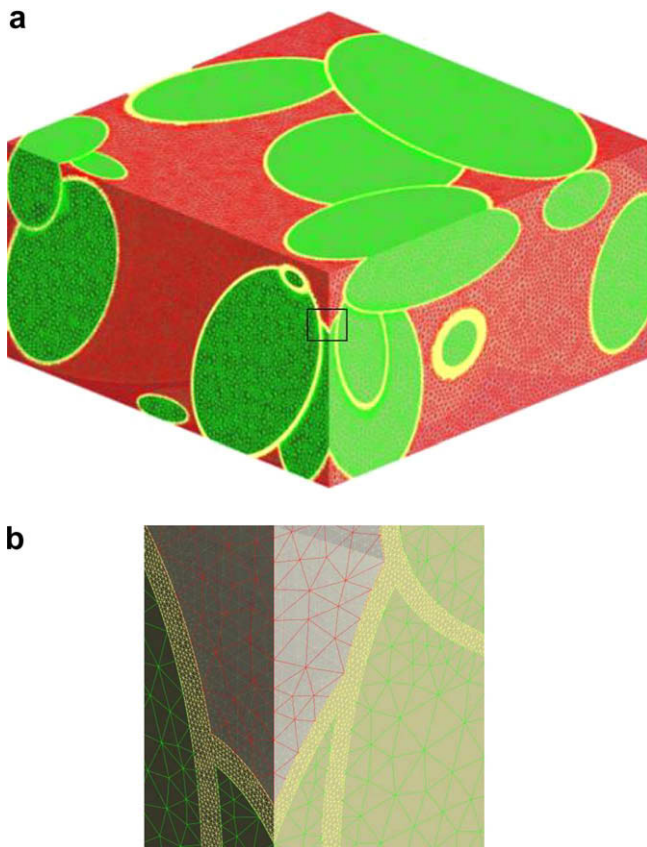


Fig. 13. The geometric model of apple parenchyma tissue (Fig. 11) in finite volume environment (ICEM, CFD) (a) and zoomed view of the cell wall (b).

4. Discussion

We obtained models of the microstructure of tissue in a format that can be used directly in computer aided design and engineering software, such as finite element and computational fluid dynamics programs. The different components can easily be assigned to different physical models to compute mechanics and mass transport. The advantage of the ellipsoid tessellation method is that small irregularities are avoided in the final model and smoothed geometry models are obtained with similar microscopic and lumped characteristics as the real tissue.

Unstructured finite element meshing of the solid model geometry was feasible. Unstructured tetrahedral meshing is preferred over regular meshes, that use one element per voxel and which are limited in accuracy to the voxel size of the original images. Mesh refinements and coarsening can be achieved more easily in our approach, than with voxel/element meshing methods already available (Maire et al., 2003). Available advanced meshing methods to avoid problems with excessively large voxel/element meshes include sub-resolution meshing, parallel computing and techniques based on Fast Fourier Transform. Sub-resolution meshing has the important drawback of causing loss of cell architecture (Maire et al., 2003). Parallel computing requires dedicated code (Barbe et al., 2001). The last method has only been applied to mechanical problems so far and convergence problems have been reported (Maire et al., 2003).

Because ellipsoid tessellation is an approximate method, the real geometry cannot be matched exactly. We found that in particular the modeled void network was somewhat different from the measured one. Verboven et al. (2008) measured void fractions of $23.0 \pm 4.0\%$ for apple and $5.1 \pm 1.5\%$ for pear parenchyma, respectively, on cubic sample sizes up to a few mm^3 . The tessellation algorithm yielded smaller apple parenchyma porosity and larger pear parenchyma porosity. This can mainly be attributed to the small sample size under consideration. We demonstrated before the importance of a sufficiently large representative volume element to calculate lumped properties such as void fraction (Mendoza et al., 2007; Mebatsion et al., 2008a), based on measurements. When the volume becomes too small, the void fraction may deviate from the characteristic tissue value and the standard deviation increases. Here we have demonstrated that void fraction may increase (for the pear samples), or decrease (for the apple samples) at too low a sample size.

In addition to size, connectivity of the voids is extremely important for mass transfer. Connectivity determines the tortuosity of the void channels, which are the main pathways for gas exchange. Effective diffusivity is inversely proportional to the tortuosity of the pathways and scales with void fraction (Datta, 2002). The new geometry models support the hypothesis that differences in effective diffusivity between fruits is related to tissue microstructure (Verboven et al., 2008; Ho et al., 2008). Here we have shown that our tessellation correctly reproduces void connectivity differences between tissues. In addition, the models supply connectivity values for the symplastic pathway.

Fruits are composed of different tissues (Verboven et al., 2008). In particular, the skin layers are important for both mass transfer and fruit mechanics. In this region cells are patterned in apple without significant void fraction. In pear, smaller cells than cortex cells are found, but the architecture is similar to the cortex with limited void fraction. Both tissue structures should be reproducible with the current method. In the pear cortex, we also find specific stone cell structures, clustered small cells with thickened cell walls that render the typical grainy texture of pears. Around these dead structures, cells are extremely stretched during cell growth. The tessellation method should be easily applied to such structures, however, because the ellipsoid cell shapes are preserved. In the core region of pears, and in throughout the cortex of apple, vascular bundles are present. The xylem vessels, mostly void after harvest, are surrounded by densely packed phloem cells. In particular the vessels that are grouped in bundles of 10–30, will require a different modeling approach.

5. Conclusions and future direction

Ellipsoid tessellation of fruit cortex tissue produced cell architectures very similar to measured tissue structures of the pear

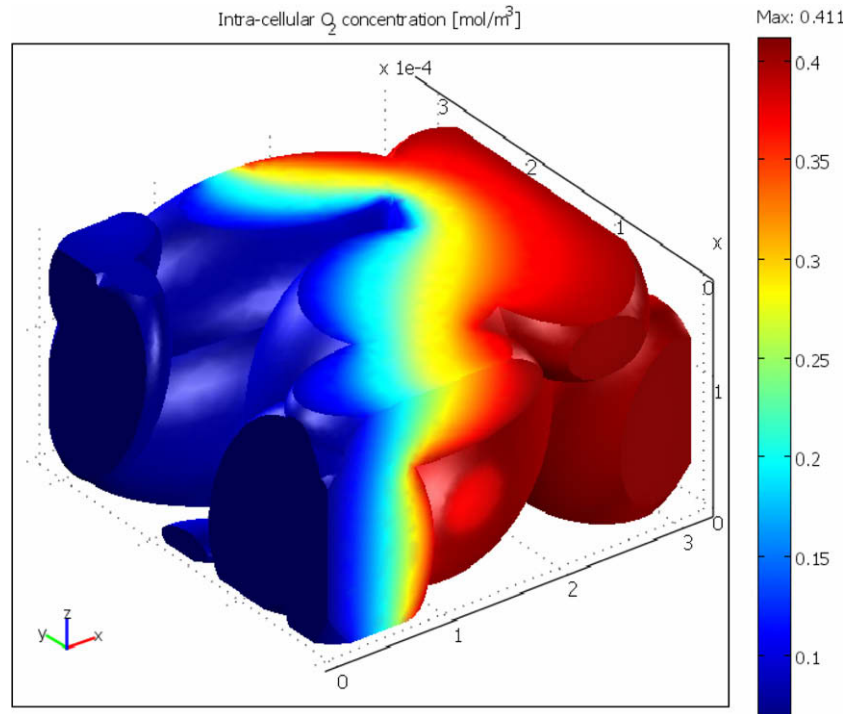


Fig. 14. The oxygen concentration profile inside cells using finite element simulations (COMSOL multiphysics, Stockholm, Sweden). The oxygen transport was caused by the partial pressure across the boundaries of the tissue. The partial pressure and concentration inside the tissue was related by the universal ideal gas law.

and apple cortex. The mathematical model that is used to generate the tissue geometry is generic. Provided the spatio-statistical properties of the tissue are known, the method can be readily used to produce virtual tissue models using the statistical distributions. The resulting microstructural features composing the symplast, cell walls and void space can be readily quantified and used in general finite element software, without particular efforts. It is expected that most of the other fruit tissues can be readily modeled by means of ellipsoid tessellation.

The geometric representation of the fruit microstructure is the founding component of multiscale modeling of transport phenomena and mechanical deformation of fruits (using microscale simulations to investigate macroscale effects), and widens our knowledge about fruit–environment interactions and the evolution of physiological disorders such as wooliness in nectarines, hollow heart in potatoes, water core in apples, spongy tissue in mango and core break down and internal browning in pear tissue. Finally, the use of these models will lead to improved cool room design and control.

Ellipsoid tessellation geometries can be used in finite element simulations to study the transport mechanisms of gas and moisture across the cells and inside intercellular spaces to have a clear understanding of the physiological disorders inside a fruit tissue. Fig. 14 shows the simulation of the oxygen profile inside the cells. The result is meant to show the potential of the model geometry to be used in finite element simulations.

Acknowledgements

Financial support by the Flanders Fund for Scientific Research (FWO-Vlaanderen) (Project G.0200.02) and the K.U. Leuven (Research council scholarship for H.K. Mebatsion and IRO PhD scholarship for Q.T. Ho) are gratefully acknowledged. Synchrotron experiments were conducted at ESRF in Grenoble, France. Pieter Verboven is Fellow of the Industrial Research Fund of the K.U. Leuven.

References

- Barbe, F., Decker, L., Jeulin, D., Cailletaud, G., 2001. Intergranular and intragranular behavior of polycrystalline aggregates. Part 1: F.E. model. *International Journal of Plasticity* 17 (4), 513–536.
- Celia, M., Reeves, P., Ferrand, L., 1995. Recent advances in pore scale models for multiphase flow in porous media. *Review of Geophysics Supplement* 33, 1049–1057.
- Chaplain, M.A.J., 1993. The strain energy function of an ideal plant cell wall. *Journal of Theoretical Biology* 163, 77–97.
- Cloetens, P., Ludwig, W., Baruchel, J., Van Dyck, D., Van Landuyt, J., Guigay, J.P., Schlenker, M., 1999. Holotomography: quantitative phase tomography with micrometer resolution using hard synchrotron radiation X rays. *Applied Physics Letters* 75, 2912–2914.
- Datta, A.K., 2002. *Biological and Bioenvironmental Heat and Mass Transfer*. CRC Press, Taylor and Francis Group, Boca Raton, Florida, ISBN 0-8247-0775-3. 383 pp.
- Denison, R.F., 1992. Mathematical modelling of oxygen diffusion and respiration in legume root nodules. *Plant Physiology* 98, 901–907.
- Dražeta, L., Lang, A., Alistair, J.H., Richard, K.V., Paula, E.J., 2004. Air volume measurement of 'Braeburn' apple fruit. *Journal of Experimental Botany* 55, 1061–1069.
- Harker, F.R., Ferguson, I.B., 1988. Calcium ion transport across discs of the cortical flesh of apple fruit in relation to fruit development. *Physiologia Plantarum* 74, 695–700.
- Ho, Q.T., Verboven, P., Verlinden, B.E., Lammertyn, J., Vandewalle, S., et al., 2008. A continuum model for metabolic gas exchange in pear fruit. *PLoS Computational Biology* 4 (3), e1000023. doi:10.1371/journal.pcbi.1000023.
- Ho, Q.T., Verlinden, B.E., Verboven, P., Nicolai, B.M., 2006. Gas diffusion properties at different positions in the pear. *Postharvest Biology and Technology* 41, 113–120.
- Jackman, R.L., Stanley, D.W., 1995. Perspectives in the textural evaluation of plant food. *Trends in Food Science and Technology* 6, 187–194.
- Kuroki, S., Oshita, S., Sotome, I., Kawagoe, Y., Seo, Y., 2004. Visualization of 3-D network of gas-filled intercellular spaces in cucumber fruit after harvest. *Postharvest Biology and Technology* 33, 255–262.
- Lee, S.J., Saravanan, R.S., Damasceno, C. M.B., Yamane, H., Kim, B.D., Rose, J.K.C., 2004. Digging deeper in to the plant cell wall proteome. *Plant Physiology and Biochemistry* 42, 979–988.
- Lewicki, P.P., Pawlak, R.P., 2005. Effect of osmotic dewatering on apple tissue structure. *Journal of Food Engineering* 66, 43–50.
- Maire, E., Fazekas, A., Salvo, L., Dendievel, R., Youssef, S., Cloetens, P., Letang, J.M., 2003. X-ray tomography applied to the characterization of cellular materials. Related finite element modeling problems. *Composites Science and Technology* 63, 2431–2443.

- Mebatsion, H.K., Verboven, P., Ho, Q.T., Verlinden, B.E., Nicolai, B.M., 2008a. Modelling fruit (micro) structure, why and how? *Trends in Food Science and Technology* 19, 59–66.
- Mebatsion, H.K., Verboven, P., Jancsó, P.T., Ho, Q.T., Verlinden, B., Nicolai, B.M., 2008b. Modeling 3-D fruit tissue microstructure using a novel ellipsoid tessellation algorithm. *CMES – Computer Modelling in Engineering and Sciences* 29 (3), 137–149.
- Mebatsion, H.K., Verboven, P., Verlinden, B.E., Ho, Q.T., Nguyen, T.A., Nicolai, B.M., 2006. Microscale modelling of fruit tissue using Voronoi tessellations. *Computers and Electronics in Agriculture* 52, 36–48.
- Mendoza, F., Verboven, P., Mebatsion, H.K., Kerckhofs, G., Wevers, M., Nicolai, B.M., 2007. Three-dimensional pore space quantification of apple tissue using X-ray computed microtomography. *Planta* 226 (3), 559–570.
- Rajapakse, N.C., Banks, N.H., Hewett, E.W., Cleland, D.J., 1990. Development of oxygen concentration gradients in flesh tissues of bulky plant organs. *Journal of American Society of Horticultural Science* 115, 793–797.
- Verboven, P., Kerckhofs, G., Mebatsion, H.K., Ho, Q.T., Temst, K., Wevers, M., Cloetens, P., Nicolai, B.M., 2008. 3-D gas exchange pathways in pome fruit characterised by synchrotron X-ray computed tomography. *Plant Physiology* 147, 518–527.
- Yamaki, S., Ino, M., 1992. Alteration of cellular compartmentation and membrane permeability to sugars in immature and mature apple fruit. *Journal of American Society of Horticultural Science* 117, 951–954.
- Zhong, R., Ye, Z.H., 2007. Regulation of cell wall biosynthesis. *Current Opinion in Plant Biology* 10, 564–572.